Progress In Electromagnetics Research, Vol. 139, 145–176, 2013

DISPERSION AND DIELECTRIC EFFECTS ON REFLECTION AND TRANSMISSION OF ELECTROMAGNETIC WAVES PROPAGATING IN MULTIPLE STAGES OF TAPE-HELIX BLUMLEIN TRANSMISSION LINES

Yu Zhang and Jinliang Liu*

College of Opto-electronic Science and Engineering, National University of Defense Technology, Changsha 410073, China

Abstract—Tape-helix transmission lines and helical coils have important applications in communication technology, signal measurement, pulse delay, pulse forming and antenna technology. In this paper, a set of fully dispersive propagation theory based on matrix method is firstly introduced to explain the propagation characteristics of travelling electromagnetic waves in multiple stages of helical Blumlein transmission lines with finite lengths. The different stages of helical transmission lines are filled with different propagation dielectrics, and the effects of dispersion and dielectrics on the propagation matrix and S-parameter matrix of the travelling waves are analyzed in detail. Relations of the exciting current waves in the series-connected helical Blumlein transmission lines are studied, and the dispersive transmission coefficients and reflection coefficients of electromagnetic waves at different dielectric ports are also initially analyzed. As an innovation, the proposed fully dispersive propagation theory which was demonstrated by simulation and experiments can substitute the non-propagating tape-helix dispersion theory and the non-dispersive telegraphers' equation to analyze the helical transmission lines.

1. INTRODUCTION

Transmission line is a device which can be employed to transport and propagate electromagnetic waves in different frequency bands, and it has important applications in power system [1, 2], electromagnetic communication technology [3], signal measurement [4, 5], pulse delay and transmission [6–13], and pulsed power technology [14–16]. Usually,

Received 28 January 2013, Accepted 11 April 2013, Scheduled 23 April 2013

* Corresponding author: Jinliang Liu (ljle333@yahoo.com).

the transmission line has intrinsic power capacity and working band. From the geometric structures, the common-use transmission lines include the two-wire transmission line [1], coaxial transmission line [14, 15], isolated parallel plates [16] and microstrip lines [17]. If the dispersion characteristics are considered [18], the transmission lines can be divided into two types such as the dispersive line [14] and the non-dispersive transmission line [15, 16]. Helical transmission line is a kind of important transmission line including helical coils as the slow-wave structure, in which the phase velocities of waves can be slowed down [19]. Helical transmission line and helical coils have been widely employed in power pulse forming [14, 20, 21], high-power microwave radiation [22], high-power laser pump [23], electromagnetic pulse radiation [24], X-ray radiography, processing of industrial exhaust gas and water, food sterilization and biomedical applications [25].

In order to obtain higher transmission power or get higher voltage amplitude, the helical transmission line or pulse forming line usually adopts the Blumlein-type structure for compactness [20, 21]. That's to say, the transmission line consists of three hollow cylindrical conductors in a coaxial distribution, and the middle conductor which withstands high voltage is formed by metal tape-helix coils curling along the axial direction. The interspace of the cylindrical conductors are filled with insulated dielectric. As the transmission line has a finite length in practice, wave transmission and reflection phenomenon occurs like the optical lines when the electromagnetic waves propagate to the terminal dielectric port of the transmission line. The problems of wave propagation, transmission and reflection in multiple layers of dielectrics or at dielectric-fractal interface were concerned in reference [26, 27], but dispersion problems were not considered. Through employing the non-dispersive travelling wave propagation method based on telegraphers' equation, the transmission and reflection of the square voltage waves at different impedance ports were analyzed in detail in references [28–30] without considering the helical dispersion. Through combining the helical dispersion theory and the non-dispersive lumped circuit theory, references [31–33] calculated the parameters of tape-helix Blumlein lines, but the employed dispersion theory based on an approximation of "infinite-long line" can not analyze the wave reflection, transmission and the S-parameters at the ports of the helical transmission line with a finite length. In the MHz burst repetitive operations of accelerator and high-power pulse generator, multiple stages of helical transmission lines are used as pulse delay lines and pulse forming lines for output of a pulse string [10–13]. As the propagating waves travel through each joint port of the multiple helical lines, helical dispersion and different port dielectrics have strong effects on the propagation, transmission

and reflection of electromagnetic waves. As a result, the quality of the output pulse string of the accelerator system was also affected. The question that how these problems affect the output pulse string should be studied. However, the previous helical dispersion theory based on the approximation of 'infinite long line' in references [31–33] can not analyze these wave propagation issues and the relevant physical problems in multiple stages of helical transmission lines with finite lengths.

In this paper, the previous helical dispersion theory combining with the lumped circuit theory is improved, and a set of fully dispersive propagation theory based on matrix method is initially put forward to explain the propagation characteristics of travelling electromagnetic waves in multiple stages of helical Blumlein transmission lines with finite lengths. The focuses are on the dispersion and dielectrics effects on the wave transmission coefficients, reflection coefficients, transmission matrices and S-parameter matrices at different dielectric ports. This paper explains the relevant physics of electromagnetic waves propagation in helical transmission lines, which shows great value on the design and analysis of dispersive transmission lines and pulse delay lines.

2. TRAVELLING ELECTROMAGNETIC WAVES AND DISPERSION RELATION

Figure 1 shows the geometric structure of the m-stage (m is an integer) helical Blumlein transmission lines in series with different filling dielectrics. Cylindrical co-ordinates are established as (r, θ, z) as shown in Fig. 1, and the axial direction is z direction. Each stage of the Blumlein transmission line consists of an outer conductor, a middle helical conductor, an inner conductor and the filling dielectric for insulation. The outer radius of the inner conductor and the inner radius of the outer conductor are as r_1 and r_3 respectively. The helical conductor is formed by a tape helix curling along z direction, and the helical conductor is symmetric and periodic in the azimuthal direction (θ) and axial direction (z) respectively. As Fig. 1 shows, the tape width, pitch, helical radius and pitch angle are as δ, p, r_2 and ψ respectively. m stages of helical Blumlein transmission lines are in series along z direction, and the ith (i is an integer, $1 \leq i \leq m$) stage line is between z_{i-1} and z_i. The length of the ith stage Blumlein line is as $l_i = z_i - z_{i-1}$. In the ith stage Blumlein line, define the region where $r_1 < r < r_2$ as the inner line or region I, the region where $r_2 < r < r_3$ as the outer line or region II, as Fig. 1 shows. In the ith stage, the same dielectric fills in region I and region II, and the

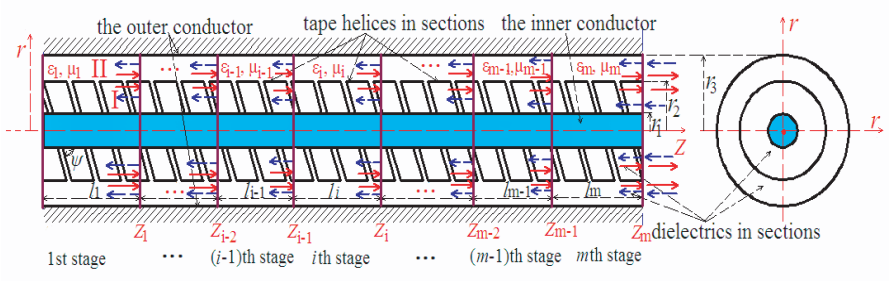

Figure 1. The series combination structure of the m-stage tape-helix transmission lines filled with m kinds of dielectrics respectively.

permittivity and permeability of the dielectric are defined as ε_i and μ_i respectively. Define the permittivity and permeability of the free space as ε_0 and μ_0.

As the m-stage helical Blumlein transmission lines have different filling dielectrics, the impedance and slow-wave characteristics of each stage are different from each other. So, wave transmission and reflection occur at z_i port. As a result, two waves including the incident wave and the reflection wave exist both region I and region II, as shown in Fig. 1. This point is quite different from the infinite long line analyzed in reference [31–33]. The traditional non-dispersive wave propagation method employs the lumped parameters such as impedances on the two sides of the z_i port to calculate the transmission coefficient and reflection coefficient of z_i port. However, the dispersion effect on these coefficients and the travelling waves can not be analyzed. When the incident electromagnetic wave is injected into the ith stage of Blumlein line, induced current flowing on the surface of the tape helix is synchronously generated by the incident wave; or in other words, when the exciting current flows through the surface of the tape helix, electromagnetic waves in region I and region II are synchronously generated. The incident wave and the reflection wave exist simultaneously, and their corresponding induced currents on the tape helix also exist simultaneously to satisfy the boundary conditions and the dispersion relation of the helical transmission line. An important recognition is obtained as that the vectorial superimpose of the incident and reflection electromagnetic waves is equivalent to the vectorial superimpose of the incident and reflection current waves; or in other words, the transmission and reflection of the electromagnetic waves is equivalent to the transmission and reflection of the exciting current waves.

In approximation, the helical tape is infinitesimally thin. The

surface current density of the tape helix consists of two components, of which one is in parallel with the helical direction ($J_{\parallel i}$) and the other is normal to the helical direction ($J_{\perp i}$). In this paper, the excitation current model in reference [34] is adopted. That is to say, 1) the amplitude of the surface current density $J_{\parallel i}$ remains the same on the tape helix, and $J_{\perp i} = 0$; 2) in the gaps between the tape turns, $J_{\parallel i} = 0$; 3) the phase constant plane of the helical surface current density is normal to the axial direction. At z_i port, the incident wave, transmission wave and reflection wave have the same angular frequency as ω. In the ith stage helical Blumlein line, the surface current density waves and electromagnetic waves consist of numerous spatial harmonics. Define the incident and reflection current density wave as $J^r_{\parallel i}$ and $J^f_{\parallel i}$, the amplitudes of the nth (n is an integer) incident and reflection spatial harmonics as $J^r_{\parallel ni}$ and $J^f_{\parallel ni}$, and the axial phase constants of the nth incident and reflection spatial harmonics as β^r_{ni} and β^f_{ni}, respectively. Obviously, $J = J^r_{\parallel i} + J^f_{\parallel i}$. As the incident wave and the reflection wave are in the same dielectric, $\beta^r_{ni} = -\beta^f_{ni}$, $\beta^r_{ni} = \beta^r_{0i} + 2\pi n/p$ and $\beta^f_{ni} = \beta^f_{0i} + 2\pi n/p$, where β^r_{0i} and β^f_{0i} are the axial phase constants of the basic (0th) incident and reflection harmonics. According to the tangential field continuity condition at z_i port, the transverse propagation constant γ_n of the nth harmonic is the same in different stages of helical lines. $J^r_{\parallel i}$ and $J^f_{\parallel i}$ can be calculated by Floquet theorem [31] as

$$\begin{cases} J^r_{\parallel i} = e^{-j\beta^r_{0i}z} \sum\limits_{n=-\infty}^{+\infty} J^r_{\parallel ni} e^{-jn(2\pi z/p - \theta - \omega t)} \\ J^r_{\parallel ni} = \dfrac{\delta J^r_{0i}}{p} e^{j(2\pi\delta/p)} \dfrac{\sin(n\pi\delta/p)}{n\pi\delta/p} \end{cases}, \quad (1)$$

$$\begin{cases} J^f_{\parallel i} = e^{-j\beta^f_{0i}z} \sum\limits_{n=-\infty}^{+\infty} J^f_{\parallel ni} e^{-jn(2\pi z/p - \theta - \omega t)} \\ J^f_{\parallel ni} = \dfrac{\delta J^f_{0i}}{p} e^{j(2\pi\delta/p)} \dfrac{\sin(n\pi\delta/p)}{n\pi\delta/p} \end{cases}.$$

In (1), t and j represent time and the unit of imaginary number, respectively. J^r_{0i} and J^f_{0i} are the amplitudes of the incident and reflection current density waves respectively. In the ith stage of helical Blumlein line filled with only one kind of dielectric, the travelling waves in region I and region II obey the same laws. Define the six field

components of the incident and reflection electromagnetic waves in region I of the ith stage line as (E^r_{1ri}, $E^r_{1\theta i}$, E^r_{1zi}, H^r_{1ri}, $H^r_{1\theta i}$, H^r_{1zi}) and (E^f_{1ri}, $E^f_{1\theta i}$, E^f_{1zi}, H^f_{1ri}, $H^f_{1\theta i}$, H^f_{1zi}), respectively; define the six field components of the incident and reflection electromagnetic waves in region II as (E^r_{2ri}, $E^r_{2\theta i}$, E^r_{2zi}, H^r_{2ri}, $H^r_{2\theta i}$, H^r_{2zi}) and (E^f_{2ri}, $E^f_{2\theta i}$, E^f_{2zi}, H^f_{2ri}, $H^f_{2\theta i}$, H^f_{2zi}), respectively. So, the slow-wave electromagnetic fields of the incident waves in region I ($r_1 < r < r_2$) and region II ($r_2 < r < r_3$) of the ith stage Blumlein line can be calculated in the same forms as shown in formula (A2) and (A3) in reference [31]. In this paper, the formulas for field components aforementioned are not provided. The axial propagation constants have relations as

$$\beta^r_{ni} = -\beta^f_{ni}, \quad (\beta^r_{ni})^2 = (\beta^f_{ni})^2 = \omega^2\varepsilon_i\mu_i + \gamma^2_n. \tag{2}$$

$J^r_{\|i}$ and $J^f_{\|i}$ independently excite electromagnetic waves travelling in the transmission line, and the total field corresponds to the vectorial superimpose of $J^r_{\|i}$ and $J^f_{\|i}$. As all the boundary conditions of the helical Blumlein transmission line are linear, the superimpose of the boundary conditions corresponds to the vectorial superimpose of the fields. As a result, the fields generated by $J^r_{\|i}$ and $J^f_{\|i}$ can independently satisfy all the boundary conditions such as

$$\begin{cases} \begin{cases} E^r_{1zi}(r_1)=0 \\ E^r_{1\theta i}(r_1)=0 \end{cases}, \begin{cases} E^f_{1zi}(r_1)=0 \\ E^f_{1\theta i}(r_1)=0 \end{cases}, \begin{cases} E^r_{2zi}(r_3)=0 \\ E^r_{2\theta i}(r_3)=0 \end{cases}, \begin{cases} E^f_{2zi}(r_3)=0 \\ E^f_{2\theta i}(r_3)=0 \end{cases} \\ E^r_{1zi}(r_2)=E^r_{2zi}(r_2), \quad E^r_{1\theta i}(r_2)=E^r_{2\theta i}(r_2), \quad E^f_{1zi}(r_2)=E^f_{2zi}(r_2), \\ E^f_{1\theta i}(r_2)=E^f_{2\theta i}(r_2) \\ H^r_{2zi}(r_2)-H^r_{1zi}(r_2)=-J^r_{\|i}\sin(\psi), \quad H^r_{2\theta i}(r_{22})-H^r_{1\theta i}(r_{21})=J^r_{\|i}\cos(\psi) \\ H^f_{2zi}(r_2)-H^f_{1zi}(r_2)=-J^f_{\|i}\sin(\psi), \quad H^f_{2\theta i}(r_{22})-H^f_{1\theta i}(r_{21})=J^f_{\|i}\cos(\psi) \\ \int_{S_i}\left(\vec{E}^r_{\|i}+\vec{E}^f_{\|i}\right)\cdot\left(\vec{J}^r_{\|i}+\vec{J}^f_{\|i}\right)^* dS_i = 0 \end{cases} \tag{3}$$

The electromagnetic coupling between the inner line and outer line of the Blumlein line is also described by (3). Through employing (3), the slow-wave harmonic coefficients (A^r_{1ni}, A^r_{2ni}, A^r_{3ni}, A^r_{4ni}) and (B^r_{1ni}, B^r_{2ni}, B^r_{3ni}, B^r_{4ni}) of the incident waves in region I and region II of the

ith stage Blumlein line can be calculated as

$$\begin{cases} \begin{cases} A^r_{2ni} = a_{1ni}A^r_{1ni},\ A^r_{4ni} = b_{1ni}A^r_{3ni} \\ a_{1ni} \triangleq -I_{n1}/K_{n1},\ b_{1ni} \triangleq -I'_{n1}/K'_{n1} \end{cases}, \\ \begin{cases} B^r_{2ni} = a_{2ni}B^r_{1ni},\ B^r_{4ni} = b_{2ni}B^r_{3ni} \\ a_{2ni} \triangleq -I_{n3}/K_{n3},\ b_{2ni} \triangleq -I'_{n3}/K'_{n3} \end{cases}, \\ B^r_{1ni} = \dfrac{I_{n2}+a_{1ni}K_{n2}}{I_{n2}+a_{2ni}K_{n2}}A^r_{1ni},\ \ B^r_{3ni} = \dfrac{I'_{n2}+b_{1ni}K'_{n2}}{I'_{n2}+b_{2ni}K'_{n2}}A^r_{3ni} \\ A^r_{3ni} = \dfrac{J^r_{\|n}\sin\psi}{(I_{n2}+b_{1ni}K_{n2}) - \dfrac{(I_{n2}+b_{2ni}K_{n2})(I'_{n2}+b_{1ni}K'_{n2})}{I'_{n2}+b_{2ni}K'_{n2}}}, \\ A^r_{1ni} = \dfrac{J^r_{\|n}\left(\cos\psi - \dfrac{\beta^r_{ni}n\sin\psi}{\gamma_n^2 r_2}\right)}{\dfrac{j\omega\varepsilon_i}{\gamma_n}\left[\dfrac{(I_{n2}+a_{1ni}K_{n2})(I'_{n2}+a_{2ni}K'_{n2})}{I_{n2}+a_{2ni}K_{n2}} - (I'_{n2}+a_{1ni}K'_{n2})\right]} \end{cases} \tag{4}$$

Of course, if the superscript 'r' is substituted by 'f' in (4), the harmonic coefficients (A^f_{1ni}, A^f_{2ni}, A^f_{3ni}, A^f_{4ni}) and (B^f_{1ni}, B^f_{2ni}, B^f_{3ni}, B^f_{4ni}) of the reflection waves in region I and region II are also obtained. In (4), I_n and K_n represent the first and the second kind of modified Bessel functions respectively. I_{n1}, I_{n2} and I_{n3} represent $I_n(\gamma_n r_1)$, $I_n(\gamma_n r_2)$ and $I_n(\gamma_n r_3)$ respectively, and K_{n1}, K_{n2} and K_{n3} obey the same rule. I'_{n2} represents the derivative of $I_n(\gamma_n r)$ on $\gamma_n r$ when $r = r_2$, so does K'_{n2}. The fields of the incident wave and reflection wave are determined by the spatial harmonic coefficients. From (4), spatial harmonic coefficients are determined by the geometric structure and the surface current density waves $J^r_{\|ni}$ and $J^f_{\|ni}$ which are restricted by the boundary conditions at z_i port.

According to the last tape-helix boundary condition shown in (3), the dispersion equation of the ith stage helical Blumlein transmission

line is obtained as

$$\begin{cases} \displaystyle\sum_{n=-\infty}^{+\infty}\left(\frac{\sin(n\pi\delta/p)^2}{(n\pi\delta/p)^2}\right) \\ \left\{\begin{array}{l} \dfrac{\gamma_n\left[\cos(\psi)-\beta_{ni}n\sin(\psi)/\left(\gamma_n^2 r_2\right)\right]^2}{\omega\varepsilon_i} \\ \dfrac{(I_{n2}K_{n1}-I_{n1}K_{n2})(I_{n2}K_{n3}-I_{n3}K_{n2})}{(I'_{n2}K_{n3}-I_{n3}K'_{n2})(I_{n2}K_{n1}-I_{n1}K_{n2})} \\ \quad -(I'_{n2}K_{n1}-I_{n1}K'_{n2})(I_{n2}K_{n3}-I_{n3}K_{n2}) \\ +\dfrac{\omega\mu_i\sin^2(\psi)}{\gamma_n} \\ \dfrac{(I'_{n2}K'_{n3}-I'_{n3}K'_{n2})(I'_{n2}K'_{n1}-I'_{n1}K'_{n2})}{(I_{n2}K'_{n3}-I'_{n3}K_{n2})(I'_{n2}K'_{n1}-I'_{n1}K'_{n2})} \\ \quad -(I_{n2}K'_{n1}-I'_{n1}K_{n2})(I'_{n2}K'_{n3}-I'_{n3}K'_{n2}) \end{array}\right\}=0 \\ especially\ n=0\colon \omega^2=\dfrac{\gamma_0^2}{\tan(\psi)^2\varepsilon_i\mu_i}\dfrac{I_{13}K_{11}-I_{11}K_{13}}{I_{03}K_{01}-I_{01}K_{03}} \end{cases} . \quad (5)$$

According to (2), $\beta_{ni}^r=-\beta_{ni}^f$ and n can be positive or negative. $\beta_{ni}n$ is the same for the incident wave and the reflection wave in (5). As a result, the incident wave and reflection wave share the same dispersion relation in the ith stage helical Blumlein line. If the radii of the ith stage helical line are different from which in other stages, the geometric parameters such as r_1, r_2, r_3, δ, p and ψ in (1)$\sim$(5) can be substituted by r_{1i}, r_{2i}, r_{3i}, δ_i, p_i and ψ_i respectively.

3. ANALYTICAL TRANSMISSION MATRIX AND *S*-PARAMETER MATRIX

The ith and the $(i+1)$th stage helical Blumlein line are on the two sides of z_i port, and the tangential field continuity conditions of dielectric surface at z_i port are as

$$\begin{cases} E_{1\theta i}^r(z_i)+E_{1\theta i}^f(z_i)=E_{1\theta(i+1)}^r(z_i)+E_{1\theta(i+1)}^f(z_i) \\ H_{1ri}^r(z_i)+H_{1ri}^f(z_i)=H_{1r(i+1)}^r(z_i)+H_{1r(i+1)}^f(z_i) \end{cases}, \\ \begin{cases} E_{1ri}^r(z_i)+E_{1ri}^f(z_i)=E_{1r(i+1)}^r(z_i)+E_{1r(i+1)}^f(z_i) \\ H_{1\theta i}^r(z_i)+H_{1\theta i}^f(z_i)=H_{1\theta(i+1)}^r(z_i)+H_{1\theta(i+1)}^f(z_i) \end{cases}. \quad (6)$$

Actually, the first two and the last two conditions in (6) are completely equivalent. The electromagnetic coupling between the two adjacent helical lines on the two sides of z_i port is also described by (6). The continuity current condition at z_i port is as

$$J^r_{\|ni} + J^f_{\|ni} = J^r_{\|n(i+1)} + J^f_{\|n(i+1)}. \tag{7}$$

Through combining (6) and (7), the crucial relations between $J^r_{\|n(i+1)}$, $J^f_{\|n(i+1)}$, $J^r_{\|ni}$ and $J^f_{\|ni}$ are obtained as

$$\begin{cases} J^r_{\|n(i+1)} = \dfrac{\varepsilon_{i+1}}{2\beta^r_{n(i+1)}}\left[\dfrac{\beta^r_{ni}}{\varepsilon_i} + \dfrac{\beta^r_{n(i+1)}}{\varepsilon_{i+1}} - \dfrac{n\tan\psi}{\gamma_n^2 r_2}\left(\dfrac{\left(\beta^r_{ni}\right)^2}{\varepsilon_i} - \dfrac{\left(\beta^r_{n(i+1)}\right)^2}{\varepsilon_{i+1}}\right.\right. \\ \left.\left. - \omega^2(\mu_i - \mu_{i+1})\right)\right] J^r_{\|ni} + \dfrac{\varepsilon_{i+1}}{2\beta^r_{n(i+1)}}\left[\dfrac{-\beta^r_{ni}}{\varepsilon_i} + \dfrac{\beta^r_{n(i+1)}}{\varepsilon_{i+1}} - \dfrac{n\tan\psi}{\gamma_n^2 r_2}\left(\dfrac{\left(\beta^r_{ni}\right)^2}{\varepsilon_i}\right.\right. \\ \left.\left. - \dfrac{\left(\beta^r_{n(i+1)}\right)^2}{\varepsilon_{i+1}} - \omega^2(\mu_i - \mu_{i+1})\right)\right] J^f_{\|ni} \\ J^f_{\|n(i+1)} = \left\{1 - \dfrac{\varepsilon_{i+1}}{2\beta^r_{n(i+1)}}\left[\dfrac{\beta^r_{ni}}{\varepsilon_i} + \dfrac{\beta^r_{n(i+1)}}{\varepsilon_{i+1}} - \dfrac{n\tan\psi}{\gamma_n^2 r_2}\left(\dfrac{\left(\beta^r_{ni}\right)^2}{\varepsilon_i} - \dfrac{\left(\beta^r_{n(i+1)}\right)^2}{\varepsilon_{i+1}}\right.\right.\right. \\ \left.\left.\left. - \omega^2(\mu_i - \mu_{i+1})\right)\right]\right\} J^r_{\|ni} + \left\{1 - \dfrac{\varepsilon_{i+1}}{2\beta^r_{n(i+1)}}\left[\dfrac{-\beta^r_{ni}}{\varepsilon_i} + \dfrac{\beta^r_{n(i+1)}}{\varepsilon_{i+1}}\right.\right. \\ \left.\left. - \dfrac{n\tan\psi}{\gamma_n^2 r_2}\left(\dfrac{\left(\beta^r_{ni}\right)^2}{\varepsilon_i} - \dfrac{\left(\beta^r_{n(i+1)}\right)^2}{\varepsilon_{i+1}} - \omega^2(\mu_i - \mu_{i+1})\right)\right]\right\} J^f_{\|ni} \end{cases}. \tag{8}$$

According to (8), the current density waves in the $(i+1)$th stage helical line are determined by the current density waves in the ith stage line. The transmission matrix of these current waves in the ith and the

$(i+1)$th stage helical Blumlein lines can be extrapolated as

$$\begin{cases} \begin{pmatrix} J^r_{\|n(i+1)} \\ J^f_{\|n(i+1)} \end{pmatrix} = \begin{pmatrix} t_{1ni} & t_{2ni} \\ t_{3ni} & t_{4ni} \end{pmatrix} \begin{pmatrix} J^r_{\|ni} \\ J^f_{\|ni} \end{pmatrix}, \quad T_{ni} \triangleq \begin{pmatrix} t_{1ni} & t_{2ni} \\ t_{3ni} & t_{4ni} \end{pmatrix} \\ t_{1ni} = \dfrac{\varepsilon_{i+1}}{2\beta^r_{n(i+1)}} \left[\dfrac{\beta^r_{ni}}{\varepsilon_i} + \dfrac{\beta^r_{n(i+1)}}{\varepsilon_{i+1}} - \dfrac{n\tan\psi}{\gamma_n^2 r_2} \left(\dfrac{\left(\beta^r_{ni}\right)^2}{\varepsilon_i} - \dfrac{\left(\beta^r_{n(i+1)}\right)^2}{\varepsilon_{i+1}} \right.\right. \\ \left.\left. -\omega^2(\mu_i - \mu_{i+1}) \right) \right] \\ t_{2ni} = \dfrac{\varepsilon_{i+1}}{2\beta^r_{n(i+1)}} \left[\dfrac{-\beta^r_{ni}}{\varepsilon_i} + \dfrac{\beta^r_{n(i+1)}}{\varepsilon_{i+1}} - \dfrac{n\tan\psi}{\gamma_n^2 r_2} \left(\dfrac{\left(\beta^r_{ni}\right)^2}{\varepsilon_i} - \dfrac{\left(\beta^r_{n(i+1)}\right)^2}{\varepsilon_{i+1}} \right.\right. \\ \left.\left. -\omega^2(\mu_i - \mu_{i+1}) \right) \right] \\ t_{3ni} = \left\{ 1 - \dfrac{\varepsilon_{i+1}}{2\beta^r_{n(i+1)}} \left[\dfrac{\beta^r_{ni}}{\varepsilon_i} + \dfrac{\beta^r_{n(i+1)}}{\varepsilon_{i+1}} - \dfrac{n\tan\psi}{\gamma_n^2 r_2} \left(\dfrac{\left(\beta^r_{ni}\right)^2}{\varepsilon_i} \right.\right.\right. \\ \left.\left.\left. - \dfrac{\left(\beta^r_{n(i+1)}\right)^2}{\varepsilon_{i+1}} - \omega^2(\mu_i - \mu_{i+1}) \right) \right] \right\} = 1 - t_{1ni} \\ t_{4ni} = \left\{ 1 - \dfrac{\varepsilon_{i+1}}{2\beta^r_{n(i+1)}} \left[\dfrac{-\beta^r_{ni}}{\varepsilon_i} + \dfrac{\beta^r_{n(i+1)}}{\varepsilon_{i+1}} - \dfrac{n\tan\psi}{\gamma_n^2 r_2} \left(\dfrac{\left(\beta^r_{ni}\right)^2}{\varepsilon_i} \right.\right.\right. \\ \left.\left.\left. - \dfrac{\left(\beta^r_{n(i+1)}\right)^2}{\varepsilon_{i+1}} - \omega^2(\mu_i - \mu_{i+1}) \right) \right] \right\} = 1 - t_{2ni} \end{cases} \quad (9)$$

In (9), t_{1ni}, t_{2ni}, t_{3ni} and t_{4ni} are the four matrix components. The current density waves ($J^r_{\|i}$ and $J^f_{\|i}$) which are composed by the numerous harmonics also can be extrapolated, according to (1). Of course, the transmission matrix (9) can also be expressed in the form of the S-parameter matrix as

$$\begin{cases} \begin{pmatrix} J^f_{\|ni} \\ J^r_{\|n(i+1)} \end{pmatrix} = \begin{pmatrix} S_{11ni} & S_{12ni} \\ S_{21ni} & S_{22ni} \end{pmatrix} \begin{pmatrix} J^r_{\|ni} \\ J^f_{\|n(i+1)} \end{pmatrix}, \; S_{ni} \triangleq \begin{pmatrix} S_{11ni} & S_{12ni} \\ S_{21ni} & S_{22ni} \end{pmatrix} \\ S_{11ni} = -\dfrac{t_{3ni}}{t_{4ni}}, \; S_{12ni} = \dfrac{1}{t_{4ni}}, \; S_{21ni} = t_{1ni} - \dfrac{t_{3ni}t_{2ni}}{t_{4ni}}, \; S_{22ni} = \dfrac{t_{2ni}}{t_{4ni}} \end{cases} \quad (10)$$

In (10), $S_{11ni} \sim S_{22ni}$ are the four matrix components which are closely related with $t_{1ni} \sim t_{4ni}$ shown in (9). According to (10),

the transmission matrix T_{n1m} of the electromagnetic waves or current density waves from the 1st stage to the mth stage line can be extrapolated as (11) by the iteration method.

$$\begin{cases} \begin{pmatrix} J^r_{\|nm} \\ J^f_{\|nm} \end{pmatrix} = T_{n(m-1)} \begin{pmatrix} J^r_{\|n(m-1)} \\ J^f_{\|n(m-1)} \end{pmatrix} = T_{n(m-1)} T_{n(m-2)} \begin{pmatrix} J^r_{\|n(m-2)} \\ J^f_{\|n(m-2)} \end{pmatrix} \\ = \ldots = T_{n(m-1)} T_{n(m-2)} \ldots T_{n1} \begin{pmatrix} J^r_{\|n1} \\ J^f_{\|n1} \end{pmatrix} \\ T_{n1m} = T_{n(m-1)} T_{n(m-2)} \ldots T_{n1} \\ = \begin{pmatrix} t_{1n(m-1)} & t_{2n(m-1)} \\ t_{3n(m-1)} & t_{4n(m-1)} \end{pmatrix} \cdots \begin{pmatrix} t_{1n1} & t_{2n1} \\ t_{3n1} & t_{4n1} \end{pmatrix} \end{cases} . \quad (11)$$

Of course, the transmission matrix of any two stages of helical lines also can easily be obtained from (11). (9) and (10) demonstrate that the four components of the transmission matrix are effected by the dispersion effect of helical transmission lines. (10) and (11) are both suitable for region I and region II of the Blumlein line.

In order to analyze the dispersion effect on the transmission matrix shown in (9), a batch of geometric parameters of the helical Blumlein transmission lines shown in Fig. 1 is provided for dispersion analysis: $r_1 = 65\,\text{mm}$, $r_2 = 100\,\text{mm}$, $r_3 = 152\,\text{mm}$, $\delta = 100\,\text{mm}$, $p = 105\,\text{mm}$ and $\psi = 80.5°$. The relative permittivity and relative permeability of the filling dielectric in the ith line are as $\varepsilon_{ri} = 81.5$ and $\mu_{ri} = 1$, and the same parameters in the $(i+1)$th line are as $\varepsilon_{r(i+1)} = 4.5$ and $\mu_{r(i+1)} = 1$. Of course, $\varepsilon_i = \varepsilon_0\varepsilon_{ri}$, $\mu_i = \mu_0\mu_{ri}$, $\varepsilon_{(i+1)} = \varepsilon_0\varepsilon_{r(i+1)}$, $\mu_{(i+1)} = \mu_0\mu_{r(i+1)}$. In Fig. 2(a), the dispersion effect on the transmission matrix component t_{1ni} is presented. To the basic harmonic ($n = 0$) of the current wave, the abscissa γ_0 increases from 0 to π/p while the wave frequency f ($f = \omega/2\pi$) synchronously increases from 0 to 27.56 MHz, according to (5). When f of the 0th harmonic varies, the fact that t_{10i} basically remains at 0.528 demonstrates that the dispersion effect on t_{10i} can be neglected. However, when γ_0 and f of the higher order harmonics ($n > 0$) synchronously increase from 0, t_{1ni} of these harmonics decreases from 1 to a level which is always much larger than $t_{10i} = 0.528$. If the harmonic number n is next to 0, t_{1ni} is much lower. The fact that higher wave frequency f corresponds to lower t_{1ni} shows the dispersion effect on the wave transmission matrix. Fig. 2(b) shows the dispersion effect on t_{2ni}, which is similar to the effect shown in Fig. 2(a). When γ_0 and f of the 0th harmonic synchronously increase from 0, t_{20i} remains at 0.472. However, when f increases from 0, t_{2ni} of the higher order harmonics decreases from 0.945, and larger n corresponds to larger t_{2ni}. t_{1ni} and t_{2ni} of the

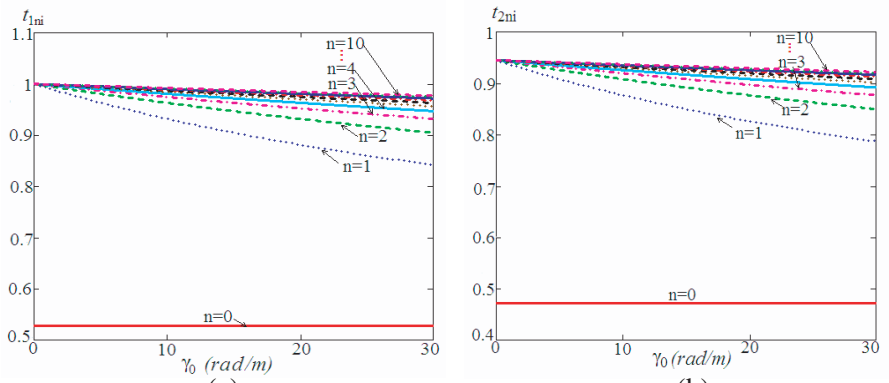

Figure 2. Dispersion effect of the tape helix on the transmission matrix of the stages of helical transmission lines in series when $\varepsilon_{ri} > \varepsilon_{r(i+1)}$; (a) Dispersion effect on t_{1ni} of the transmission matrix; (b) Dispersion effect on t_{2ni} of the transmission matrix.

minus harmonics also have similar changes in comparison with the corresponding plus harmonics, respectively. As t_{3ni} and t_{4ni} are linear to t_{1ni} and t_{2ni} respectively from (9), dispersion effects on t_{3ni} and t_{4ni} are also similar to the effects shown in Figs. 2(a) and 2(b) respectively.

Reference [31] calculated the harmonic coefficients similar to the parameters shown in (4), and the coefficients represented the proportions of the harmonics in the total field. Through combining (1), (4), (9) and (10), the dispersive transmission matrix and dispersive S-parameter matrix of the electromagnetic waves propagating in multiple stages of helical Blumlein lines are obtained. The study results from Fig. 2 reveal that the dispersion effect of helical line on the transmission of the 0th harmonic is not obvious, but the effect on higher order harmonics is intensive. In the low frequency band, the dispersion almost has the same effect on all of the transmission matrix components of the higher order harmonics. When n is large enough, the transmission matrix components have little change when f changes.

In many practical cases, the helical transmission line has its intrinsic transmission band. The lower-limit frequency of the coaxial helical transmission line is close to 0, while the upper-limit frequency is determined by the pitch p of tape helix and the radii of the Blumlein line [31, 33]. Usually, the upper-limit frequency of helical line ranges from dozens of MHz to more than hundreds of MHz. In the frequency band which is lower than dozens of MHz, the electromagnetic wave in the transmission line mainly consists of the 0th harmonic

component [31]. Through combining (2) with the second formula in (5),

$$(\beta_{0i})^2 = \gamma_0^2 \left(1 + \frac{1}{\tan(\psi)^2} \frac{I_{13}K_{11} - I_{11}K_{13}}{I_{03}K_{01} - I_{01}K_{03}}\right). \tag{12}$$

As the tangential field continuity condition at z_i port determines that γ_0 is the same in different transmission lines, (12) reveals that $\beta_{0i}^r = \beta_{0(i+1)}^r$ if the geometric parameters remain unchanged in different lines. Under the condition that the 0th harmonic is dominant at low frequency band, the transmission matrix T_{0i} can be simplified as

$$\begin{cases} \begin{pmatrix} J_{\|0(i+1)}^r \\ J_{\|0(i+1)}^f \end{pmatrix} = \begin{pmatrix} t_{10i} & t_{20i} \\ t_{30i} & t_{40i} \end{pmatrix} \begin{pmatrix} J_{\|0i}^r \\ J_{\|0i}^f \end{pmatrix}, \quad T_{0i} \triangleq \begin{pmatrix} t_{10i} & t_{20i} \\ t_{30i} & t_{40i} \end{pmatrix} \\ t_{10i} = \dfrac{1}{2}\left(1 + \dfrac{\varepsilon_{i+1}}{\varepsilon_i}\right), \quad t_{20i} = \dfrac{1}{2}\left(1 - \dfrac{\varepsilon_{i+1}}{\varepsilon_i}\right), \\ t_{30i} = \dfrac{1}{2}\left(1 - \dfrac{\varepsilon_{i+1}}{\varepsilon_i}\right) = t_{20i}, \quad t_{40i} = \dfrac{1}{2}\left(1 + \dfrac{\varepsilon_{i+1}}{\varepsilon_i}\right) = t_{10i} \end{cases}. \tag{13}$$

It is obvious that the transmission matrix is not dispersive under the dominant 0th harmonic condition. This conclusion corresponds with the results that $t_{10i} \sim t_{40i}$ remain unchanged though f changes in Fig. 2. The transmission matrix T_{0ij} $(1 \le i < j \le m)$ between the ith and the jth stage of transmission lines is presented as

$$T_{0ij} = T_{0(j-1)} T_{0(j-2)} \cdots T_{0i} = \begin{pmatrix} t_{10(j-1)} & t_{20(j-1)} \\ t_{30(j-1)} & t_{40(j-1)} \end{pmatrix} \cdots \begin{pmatrix} t_{10i} & t_{20i} \\ t_{30i} & t_{40i} \end{pmatrix}. \tag{14}$$

Though the transmission matrix T_{n1m} and the incident current density wave $J_{\|n1}^r$ is clear and fixed, the reflection current density wave $J_{\|n1}^f$ in the 1st stage line is still not clear. Actually, $J_{\|n1}^f$ is finally determined by the boundary conditions at z_m port (the terminal port).

4. TRANSMISSION CHARACTERISTICS OF ELECTROMAGNETIC WAVES UNDER SOME COMMON-USED CASES

4.1. The Length of the mth Helical Transmission Line Is Infinite Long ($l_m = \infty$)

The model that the mth $(m > 1)$ stage transmission line is infinite long means complete absorption or no reflection at the terminal port (z_m), as shown in Fig. 3. So, the boundary conditions at z_m port correspond to $J_{\|nm}^f = 0$. Through putting the condition into (9),

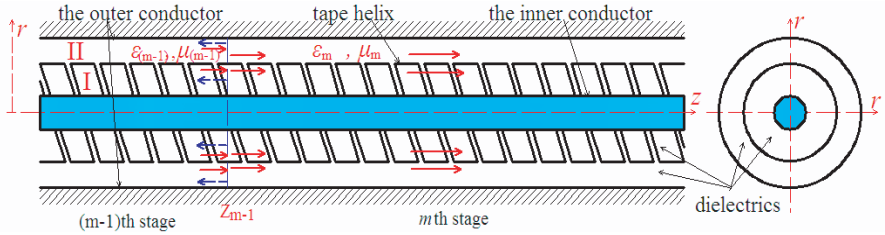

Figure 3. Geometric structure of the $(m-1)$th and the mth stage of tape-helix transmission lines in series when the mth stage line is long enough.

relations of $J^r_{\|n(m-1)}$, $J^f_{\|n(m-1)}$ and $J^r_{\|nm}$ are obtained as

$$\begin{cases} J^f_{\|n(m-1)} = \xi_{(m-1)} J^r_{\|n(m-1)}, \quad J^r_{\|nm} = \alpha_{(m-1)} J^r_{\|n(m-1)} \\ \xi_{(m-1)} \triangleq -\dfrac{t_{3n(m-1)}}{t_{4n(m-1)}}, \quad \alpha_{(m-1)} \triangleq t_{1n(m-1)} - \dfrac{t_{2n(m-1)} t_{3n(m-1)}}{t_{4n(m-1)}} \end{cases}. \quad (15)$$

In (15), $\xi_{(m-1)}$ and $\alpha_{(m-1)}$ respectively represent the reflection coefficient and transmission coefficient of the current density wave amplitude at z_{m-1} port. Actually, $\xi_{(m-1)}$ and $\alpha_{(m-1)}$ are the S parameters such as S_{11ni} and S_{21ni} in the S-parameter matrix shown in (13).

According to (11), the incident current wave and reflection wave in the 1st stage line can be obtained in turn as (16).

$$\begin{pmatrix} J^r_{\|n1} \\ J^f_{\|n1} \end{pmatrix} = \begin{pmatrix} t_{1n1} & t_{2n1} \\ t_{3n1} & t_{4n1} \end{pmatrix}^{-1} \cdots \begin{pmatrix} t_{1n(m-2)} & t_{2n(m-2)} \\ t_{3n(m-2)} & t_{4n(m-2)} \end{pmatrix}^{-1} \begin{pmatrix} 1 \\ \xi_{(m-1)} \end{pmatrix} J^r_{\|n(m-1)}. \quad (16)$$

In (16), two linear equations are included. From the first equation, $J^r_{\|n(m-1)}$ can be extrapolated by $J^r_{\|n1}$ which is already known. Secondly, from the second linear equation, $J^f_{\|n1}$ is obtain through employing $J^r_{\|n(m-1)}$, and the relation between $J^f_{\|n1}$ and $J^r_{\|n1}$ is established. Finally, according to (11) and (13), the transmission matrix and current density waves in the stages of transmission lines are fixed. From (9) and (15), an important conclusion is obtained as $\alpha_{(m-1)} - \xi_{(m-1)} = 1$ which demonstrates the law of energy conservation.

(15) only shows the transmission relation of the nth harmonic wave. However, the total current density wave $J^r_{\|i}$ or $J^f_{\|i}$ consists of numerous harmonic waves. If we consider the transmission parameters of the total current density wave, the proportion of the nth harmonic

$J_{\|ni}^{r,f}$ in the total wave $J_{\|i}^{r,f}$ should be estimated firstly. Actually, the proportions of the 0th harmonic and higher order harmonics in the total current density wave $J_{\|i}^{r,f}$ can also be calculated from the linear Equation (1). Define the normalized proportion of the wave amplitude $J_{\|ni}^{r,f}$ of the nth harmonic as $X(n)$ by using of $J_{\|0i}^{r,f}$ as the standard for normalization. $X(n) = J_{\|ni}^{r,f}/J_{\|0i}^{r,f} = \sin(n\pi\delta/p)/(n\pi\delta/p)$. Obviously, $X(0) = 1$ and $X\ (n \neq 0) \ll X(0)$, which reveals that $J_{\|ni}^{r,f}(n \neq 0)$ is so smaller than $J_{\|0i}^{r,f}$ that it can be neglected under the low-frequency condition. $X(n)$ decreases to 0 fast when δ/p increases, which demonstrates that larger tape width δ corresponds to smaller $J_{\|ni}^{r,f}(n \neq 0)$. Define the transmission coefficient and reflection coefficient of the total current density wave $J_{\|i}^{r}$ as T_w and F_w respectively. T_w and F_w can be calculated through employing $X\,(n)$ as the weighting for superimposing on $\alpha_{(m-1)}$ and $\xi_{(m-1)}$ respectively:

$$\begin{aligned} T_w(k,\gamma_0) &= \sum_{n=-k}^{k} [X(n)\alpha_{(m-1)}(k,\gamma_0)], \\ F_w(k,\gamma_0) &= \sum_{n=-k}^{k} [X(n)\xi_{(m-1)}(k,\gamma_0)]. \end{aligned} \tag{17}$$

In (17), k ($k \geq 0$) is an integer which is large enough to get close to $+\infty$. As k is large enough, T_w and F_w can be viewed as the sum effect of all the harmonics.

Some analyses on (15) are presented as follows to describe the dispersion effect on the transmission matrix. The same geometric parameters shown in Fig. 1 are as $r_1 = 65\,\text{mm}$, $r_2 = 100\,\text{mm}$, $r_3 = 152\,\text{mm}$, $\delta = 100\,\text{mm}$, $p = 105\,\text{mm}$ and $\psi = 80.5°$. The dielectric parameters are as $\varepsilon_{r(m-1)} = 81.5$, $\mu_{r(m-1)} = 1$, $\varepsilon_{rm} = 4.5$, $\mu_{rm} = 1$, and $\varepsilon_{r(m-1)} \gg \varepsilon_{rm}$. Fig. 4(a) shows the helical dispersion effect on the current reflection coefficient $\xi_{(m-1)}$ at z_{m-1} port. Obviously, $\xi_{(m-1)}$ of the 0th harmonic wave is almost a constant at -0.895 which is next to -1. The fact that $\xi_{(m-1)}$ does not change with γ_0 and f demonstrates the dispersion has little effect on the transmission of the 0th harmonic. However, the dispersion has strong effect on the reflection coefficient of the higher order harmonics. When γ_0 and f increases, $\xi_{(m-1)}$ decreases in large scales but $|\xi_{(m-1)}|$ increases in large scales. The phenomenon reveals that most of the basic harmonic reflects but the main part of the higher order harmonic transmits rather than reflects. Higher f enhances the proportion of the reflection part of the nth harmonic, and

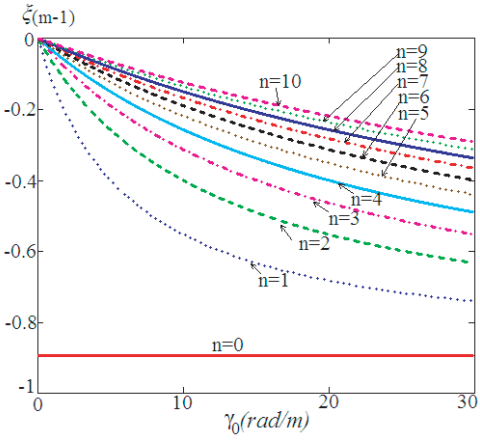

Figure 4. Dispersion effect of the tape helix on the reflection coefficient $\xi_{(m-1)}$ of the two stages of helical transmission lines in series when $\varepsilon_{r(m-1)} > \varepsilon_{rm}$.

the reflection part becomes larger when n decreases to a level close to 0. As $\alpha_{(m-1)} = \xi_{(m-1)} + 1$, the dispersion has similar effects on $\alpha_{(m-1)}$ of the higher order harmonics. $\xi_{(m-1)}$ and $\alpha_{(m-1)}$ of the minus harmonics also have similar changes in comparison with the corresponding plus harmonics, respectively.

In summary, dispersion analysis demonstrates: 1) the reflection coefficient $\xi_{(m-1)}$ (or S_{11ni}) and the transmission coefficient $\alpha_{(m-1)}$ (or S_{21ni}) at z_{m-1} port are both immune to the dispersion effect; 2) when f of the wave increases, reflection effect of wave is strengthened while the transmission effect is weakened at z_{m-1} port, under the condition $\varepsilon_{r(m-1)} > \varepsilon_{rm}$; 3) when $|n|$ increases, $|\xi_{(m-1)}|$ decreases and $|\alpha_{(m-1)}|$ increases, under the condition $\varepsilon_{r(m-1)} > \varepsilon_{rm}$. Under the high-frequency condition, many physical problems and phenomena can be explored and analyzed by the proposed dispersive transmission theory for travelling waves, rather than the traditional non-dispersive transmission theory. This point shows the value of the proposed theory in this paper.

As the dominant basic harmonic ($n = 0$) condition is suitable for many transmission lines when the wave frequency is not high enough, the reflection and transmission coefficients at z_{m-1} port are analyzed

in detail as follows. According to (15),

$$\begin{cases} J^f_{\|0(m-1)} = \xi_{(m-1)} J^r_{\|0(m-1)}, \quad J^r_{\|0m} = \alpha_{(m-1)} J^r_{\|0(m-1)} \\ \xi_{(m-1)} \triangleq -\dfrac{t_{30(m-1)}}{t_{40(m-1)}} = \dfrac{\varepsilon_m \beta^r_{0(m-1)} - \varepsilon_{(m-1)} \beta^r_{0m}}{\varepsilon_m \beta^r_{0(m-1)} + \varepsilon_{(m-1)} \beta^r_{0m}}, \\ \alpha_{(m-1)} \triangleq \left(t_{10(m-1)} - \dfrac{t_{20(m-1)} t_{30(m-1)}}{t_{40(m-1)}} \right) \\ = \dfrac{2\varepsilon_m \beta^r_{0(m-1)}}{\varepsilon_m \beta^r_{0(m-1)} + \varepsilon_{(m-1)} \beta^r_{0m}} = S_{21(m-1)} \end{cases} . \tag{18}$$

Obviously, (18) also demonstrates that $\alpha_{(m-1)} - \xi_{(m-1)} = 1$. In this paper, (18) is adequate to describe the wave transmission and reflection characteristics in multiple stages of helical lines. In comparison with the relevant classical conclusions obtained from the classical non-dispersive propagation theory used in [28–30], the transmission and reflection coefficients described by impedances are also extrapolated from the proposed dispersive propagation theory. In line with the method used in [32, 33], the axial travelling current wave I_{0zi} in the ith stage transmission line can be calculated by integrating the azimuthal magnetic field component along the surface of the tape helix; furthermore, the characteristic impedance Z_i of the ith stage helical line can also be extrapolated as (19).

$$\begin{aligned} I^{r,f}_{0zi} &= \frac{-2\pi r_2 (I_{12} - a_{10i} K_{12}) \cos(\psi)}{\frac{(I_{12} - a_{20i} K_{12})(I_{02} + a_{10i} K_{02})}{I_{02} + a_{20i} K_{02}} - (I_{12} - a_{10i} K_{12})} J^{r,f}_{\|0i}, \\ Z_i &= \frac{I_{02} + a_{10i} K_{02}}{2\pi r_2 \omega (I_{12} - a_{10i} K_{12})} \frac{1}{\varepsilon_i \beta_{0i}}. \end{aligned} \tag{19}$$

In the first formula in (19), the axial incident current wave I^r_{0zi} and the axial reflection current wave I^f_{0zi} relate to the current density wave $J^r_{\|0i}$ and $J^f_{\|0i}$ respectively. In the second formula in (19), β_{0i} can be substituted by $\beta^r_{0(m-1)}$, $\beta^f_{0(m-1)}$ and β^r_{0m} for calculating the impedances which correspond to $I^r_{0z(m-1)}$, $I^f_{0z(m-1)}$ and I^r_{0zm} respectively. As $\beta^r_{0(m-1)} = -\beta^f_{0(m-1)}$, the impedances corresponding to $I^r_{0z(m-1)}$ and $I^f_{0z(m-1)}$ have different polarities. When the wave frequency is not high enough, $\beta^r_{0(m-1)} = \beta^r_{0m}$ is true under the dominant basic harmonic condition aforementioned. Moreover, the tangential field continuity conditions at z_{m-1} port determine that $\gamma_{0(m-1)} = \gamma_{0m} = \gamma_0$. As a result, impedances in different stages

of transmission lines can be differentiated by different permittivities of the dielectrics. According to (19), $\varepsilon_{(m-1)}\beta^r_{0(m-1)} = \varepsilon_{(m-1)}\beta^r_{0m} \propto (Z_{(m-1)})^{-1}$, $\varepsilon_m\beta^r_{0m} = \varepsilon_m\beta^r_{0(m-1)} \propto (Z_m)^{-1}$. So, $\xi_{(m-1)}$ and $\alpha_{(m-1)}$ shown in (18) can also be expressed as

$$\begin{aligned} \xi_{(m-1)} &= \frac{(1/Z_m) - (1/Z_{(m-1)})}{(1/Z_m) + (1/Z_{(m-1)})} = \frac{Z_{(m-1)} - Z_m}{Z_{(m-1)} + Z_m}, \\ \alpha_{(m-1)} &= \frac{2(1/Z_m)}{(1/Z_m) + (1/Z_{(m-1)})} = \frac{2Z_{(m-1)}}{Z_{(m-1)} + Z_m}. \end{aligned} \tag{20}$$

In order to comparing with the conclusions from the classical non-dispersive theory of transmission line, the incident voltage wave $U^r_{0(m-1)}$, reflection voltage wave $U^f_{0(m-1)}$ and the transmission voltage wave U^r_{0m} are also calculated. As $U^r_{0(m-1)} = I^r_{0z(m-1)}Z_{(m-1)}$, according to (20),

$$I^r_{0z(m-1)}\frac{I_{02} + a_{10i}K_{02}}{2\pi r_2\omega(I_{12} - a_{10i}K_{12})} = \varepsilon_{(m-1)}\beta^r_{0(m-1)}U^r_{0(m-1)}. \tag{21}$$

$U^f_{0(m-1)}$ and U^r_{0m} can be extrapolated as

$$\begin{cases} U^r_{0m} = I^r_{0zm}Z_m = I^r_{0z(m-1)}\alpha_{(m-1)}Z_m \\ \quad \approx \dfrac{2\varepsilon_{(m-1)}\beta^r_{0m}}{\varepsilon_{(m-1)}\beta^r_{0m} + \varepsilon_m\beta^r_{0(m-1)}}U^r_{0(m-1)} = \dfrac{2Z_m}{Z_{(m-1)} + Z_m}U^r_{0(m-1)} \\ U^f_{0(m-1)} = I^f_{0z(m-1)}Z_{(m-1)} = -I^r_{0z(m-1)}\xi_{(m-1)}Z_{(m-1)} \\ \quad \approx \dfrac{\varepsilon_{(m-1)}\beta^r_{0m} - \varepsilon_m\beta^r_{0(m-1)}}{\varepsilon_{(m-1)}\beta^r_{0m} + \varepsilon_m\beta^r_{0(m-1)}}U^r_{0(m-1)} = \dfrac{Z_m - Z_{(m-1)}}{Z_{(m-1)} + Z_m}U^r_{0(m-1)} \end{cases}. \tag{22}$$

Define the reflection coefficient and transmission coefficient of the voltage waves as $\xi_{u(m-1)}$ and $\alpha_{u(m-1)}$.

$$\xi_{u(m-1)} = \frac{Z_m - Z_{(m-1)}}{Z_{(m-1)} + Z_m}, \quad \alpha_{u(m-1)} = \frac{2Z_m}{Z_{(m-1)} + Z_m}. \tag{23}$$

(23) shows the classical results of non-dispersive propagation theory. From (23), $\alpha_{u(m-1)} = \xi_{u(m-1)} + 1$, which corresponds with the results from (18). As (20) and (23) are obtained under low frequency conditions, the proposed dispersive propagation theory corresponds to the classical non-dispersive propagation theory. It also demonstrates that the proposed theory in this paper is more fundamental and essential for dispersion transmission lines.

4.2. The mth Helical Transmission Line Equates to An Open Circuit

A common used case is that the terminal port of the transmission line is open. In this section, the case that the entire mth stage line plays as the open circuit is analyzed in detail. That's to say, when the mth stage line is open, $Z_m = \infty$ or $Z_{m-1} \ll Z_m$. The open boundary conditions at z_{m-1} port are as

$$\begin{cases} E^r_{1\theta(m-1)}(z_{(m-1)}) + E^f_{1\theta(m-1)}(z_{(m-1)}) \\ = E^r_{1\theta m}(z_{(m-1)}) + E^f_{1\theta m}(z_{(m-1)}) \\ E^r_{1r(m-1)}(z_{(m-1)}) + E^f_{1r(m-1)}(z_{(m-1)}) \\ = E^r_{1rm}(z_{(m-1)}) + E^f_{1rm}(z_{(m-1)}) \\ H^r_{1r(m-1)}(z_{(m-1)}) + H^f_{1r(m-1)}(z_{(m-1)}) = 0 \\ = H^r_{1rm}(z_{(m-1)}) + H^f_{1rm}(z_{(m-1)}) \\ H^r_{1\theta(m-1)}(z_{(m-1)}) + H^f_{1\theta(m-1)}(z_{(m-1)}) = 0 \\ = H^r_{1\theta m}(z_{(m-1)}) + H^f_{1\theta m}(z_{(m-1)}) \end{cases} . \tag{24}$$

According to the last two conditions in (24), the integration of the tangential magnetic field at z_{m-1} port also equates to 0. As a result, $J^r_{\parallel n(m-1)} + J^f_{\parallel n(m-1)} = 0 = J^r_{\parallel nm} + J^f_{\parallel nm}$, so that $J^f_{\parallel n(m-1)} = -J^r_{\parallel n(m-1)}$ and $J^f_{\parallel nm} = -J^r_{\parallel nm}$. When the mth stage line is infinite long, no reflection wave exists so that $J^f_{\parallel nm} = 0 = J^r_{\parallel nm}$. As the mth stage line only has the incident wave $J^r_{\parallel nm}$, $\alpha_{u(m-1)}$ and $\xi_{u(m-1)}$ at z_{m-1} port can be calculated as

$$\xi_{(m-1)} = -1, \quad \alpha_{(m-1)} = 0. \tag{25}$$

(25) proves that the current wave or electromagnetic wave completely reflects at z_{m-1} port.

The broad-sense open condition $Z_{m-1} \ll Z_m$ can be transformed as $\varepsilon_{(m-1)}\beta_{0(m-1)} \gg \varepsilon_m\beta_{0m}$, according to (19). Under the dominant basic harmonic condition at low frequency band, the condition $\beta^r_{0(m-1)} = \beta^r_{0m}$ is still satisfied. So, the broad-sense open condition can be further transformed as $\varepsilon_{(m-1)}\beta_{0m} \gg \varepsilon_m\beta_{0(m-1)}$ or $\varepsilon_{(m-1)} \gg \varepsilon_m$. Obviously, the case that $\varepsilon_{r(m-1)} = 81.5 \gg \varepsilon_{rm} = 4.5$ in Fig. 4 satisfies the broad-sense open condition, and the results $\xi_{(m-1)} = -0.895$ and $\alpha_{(m-1)} = 0.105$ are close to the results shown in (25) respectively. When the broad-sense open condition is considered in (22),

$$\xi_{u(m-1)} = 1, \quad \alpha_{u(m-1)} = 2. \tag{26}$$

(26) shows that the transmission voltage at z_{m-1} port is twice as the voltage in the $(m-1)$th stage line under the open condition. (25) and (26) demonstrate that the proposed dispersive propagation theory basically equates to the classical non-dispersive propagation theory at low frequency band. Even if the mth stage line is substituted by the free space at z_{m-1} port, conditions such as (25), (26) and the broad-sense open condition still work.

4.3. The mth Helical Transmission Line Equates to a Short Circuit

Another common used case is the short circuit case. If $Z_m = 0$ or $Z_{m-1} \gg Z_m$, the mth stage line equates to a short circuit. From the general boundary conditions shown in (6), the short boundary conditions at z_{m-1} port can be improved as

$$\begin{cases} E^r_{1\theta(m-1)}(z_{(m-1)}) + E^f_{1\theta(m-1)}(z_{(m-1)}) = 0 = E^r_{1\theta m}(z_{(m-1)}) \\ + E^f_{1\theta m}(z_{(m-1)}) \\ E^r_{1r(m-1)}(z_{(m-1)}) + E^f_{1r(m-1)}(z_{(m-1)}) = 0 = E^r_{1rm}(z_{(m-1)}) \\ + E^f_{1rm}(z_{(m-1)}) \\ H^r_{1r(m-1)}(z_{(m-1)}) + H^f_{1r(m-1)}(z_{(m-1)}) = H^r_{1rm}(z_{(m-1)}) \\ + H^f_{1rm}(z_{(m-1)}) \\ H^r_{1\theta(m-1)}(z_{(m-1)}) + H^f_{1\theta(m-1)}(z_{(m-1)}) = H^r_{1\theta m}(z_{(m-1)}) \\ + H^f_{1\theta m}(z_{(m-1)}) \end{cases} . \quad (27)$$

When the mth stage line is infinite long, $J^f_{\|nm} = 0$. The broad-sense short circuit condition $Z_{m-1} \gg Z_m$ also can be transformed to $\varepsilon_{(m-1)}\beta_{0(m-1)} \ll \varepsilon_m\beta_{0m}$, according to (19). Under the dominant basic harmonic condition at low frequency band, $\beta^r_{0(m-1)} = \beta^r_{0m}$. The broad-sense short circuit condition is approximately expressed as $\varepsilon_{(m-1)}\beta_{0m} \ll \varepsilon_m\beta_{0(m-1)}$ or $\varepsilon_{r(m-1)} \ll \varepsilon_{rm}$. Through combining (18), (22) and the broad-sense short circuit condition, $\alpha_{u(m-1)}$ and $\xi_{u(m-1)}$ at z_{m-1} port can be calculated as

$$\xi_{(m-1)} = 1, \quad \alpha_{(m-1)} = 2; \quad \xi_{u(m-1)} = -1, \quad \alpha_{u(m-1)} = 0. \quad (28)$$

(28) also demonstrates that the proposed dispersive propagation theory corresponds to the classical non-dispersive propagation theory at low frequency band.

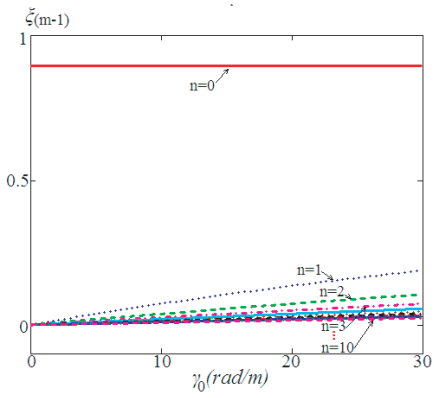

Figure 5. Dispersion effect of the tape helix on the reflection coefficient $\xi_{(m-1)}$ of the two stages of helical transmission lines in series when $\varepsilon_{r(m-1)} < \varepsilon_{rm}$.

Set the geometric parameters in Fig. 1 as $r_1 = 65\,\text{mm}$, $r_2 = 100\,\text{mm}$, $r_3 = 152\,\text{mm}$, $\delta = 100\,\text{mm}$, $p = 105\,\text{mm}$ and $\psi = 80.5°$. The dielectric parameters are set as $\varepsilon_{r(m-1)} = 4.5$, $\mu_{r(m-1)} = 1$, $\varepsilon_{rm} = 81.5$, $\mu_{rm} = 1$, and $\varepsilon_{r(m-1)} \ll \varepsilon_{rm}$. The dispersion effect on $\xi_{(m-1)}$ is shown in Fig. 5. As $\alpha_{(m-1)} = \xi_{(m-1)} + 1$, $\alpha_{(m-1)}$ has similar changes in comparison with $\xi_{(m-1)}$. When γ_0 and f change in a large scale, $\xi_{(m-1)}$ and $\alpha_{(m-1)}$ of the basic harmonic (0th) almost remain at 0.895 and 1.895, which are close to 1 and 2 respectively. Dispersion also has little effect on the reflection and transmission of the 0th harmonic under the broad-sense short circuit condition $\varepsilon_{r(m-1)} \ll \varepsilon_{rm}$. However, dispersion has strong effects on $\xi_{(m-1)}$ and $\alpha_{(m-1)}$ of the higher order harmonics. When γ_0 and f increase in a large scale, $\xi_{(m-1)}$ and $\alpha_{(m-1)}$ of the nth ($|n| > 0$) harmonic also increase. When $|n|$ gets close to 0, $\xi_{(m-1)}$ and $\alpha_{(m-1)}$ is even large. To the nth ($|n| > 0$) harmonic, $\xi_{(m-1)}$ and $\alpha_{(m-1)}$ are close to 0 and 1 respectively.

4.4. Impedance Matching Case of the mth and $(m-1)$th Helical Transmission Lines

If the impedances of the $(m-1)$th and the mth transmission line match with each other, $Z_{m-1} = Z_m$. If the geometric parameters of the two lines are the same, the impedance matching condition is equivalent to $\varepsilon_{(m-1)}\beta_{0(m-1)} = \varepsilon_m\beta_{0m}$, according to (19). In view of that $\beta^r_{0(m-1)} = \beta^r_{0m}$ under low-frequency condition, the impedance matching condition requires that $\varepsilon_{(m-1)} = \varepsilon_m$. According to (18) and (22), the reflection coefficients and transmission coefficients of the

current waves and voltage waves are as

$$\xi_{(m-1)} = 0, \quad \alpha_{(m-1)} = 1; \quad \xi_{u(m-1)} = 0, \quad \alpha_{u(m-1)} = 1. \tag{29}$$

(29) shows that the waves completely transmit from the $(m-1)$th line to the mth line. If the mth transmission line is substituted by a load impedance at z_{m-1} port, the impedance matching condition of the $(m-1)$th line is still satisfied, and relevant results still work.

5. *S*-PARAMETER SIMULATION AT THE JOINT PORT OF HELICAL TRANSMISSION LINES IN SERIES

In order to demonstrate the correctness of the transmission matrix and S-parameter matrix of multiple stages of helical Blumlein transmission lines in series, CST Microwave Studio is employed to simulate the transmission characteristics of the travelling waves in two stages of Blumlein lines in series. The simulation model is shown in Fig. 6(a), in which $r_1 = 65\,\text{mm}$, $r_2 = 100\,\text{mm}$, $r_3 = 152\,\text{mm}$, $\delta = 100\,\text{mm}$, $p = 105\,\text{mm}$ and $\psi = 80.5^\circ$. The lengths of the $(m-1)$th stage and the mth stage line are set as $l_{m-1} = l_m = 0.7\,\text{m}$. The impedances of the inner and outer lines of the mth stage Blumlein line are both about $32\,\Omega$. In order to simulate and analyze the impedance mismatching case at z_{m-1} port, set the dielectric parameter of the $(m-1)$th stage line as $\varepsilon_{r(m-1)} = 100$ and $\mu_{r(m-1)} = 1$, the dielectric parameter of the mth stage line as $\varepsilon_{rm} = 20$ and $\mu_{rm} = 1$. Discrete current ports such as Port 1, Port 2 and Port 3 are set between the tape helix and the inner line at $z = z_{m-2}$, $z = z_{m-1}$ and $z = z_m$, respectively.

At Port 1 which plays as the exciting port, the positive current direction is from the tape helix to the inner conductor, as shown in Fig. 6(a). Port 2 and Port 3 are both impedance ports, and their positive directions are both from the tape helix to the inner conductor. Impedances of Port 2 and Port 3 are both set as $32\,\Omega$ which matches with the impedance of the inner line $(r_1 < r < r_2)$ of the mth stage helical Blumlein transmission line. Quasi-square current pulse is set at Port 1 as the exciting signal, with amplitude of 1 A, pulse rise time and fall time both of 10 ns, and flat top time of 110 ns. The exciting current at Port 1 travels through the two stages of lines and electromagnetic waves are simultaneously generated. As the impedance of Port 2 match with the impedance of the inner line $(r_1 < r < r_2)$ of the mth stage line, Port 2 almost has no effect on the wave transmission at the place that $z = z_{m-1}$. In order to simulate the infinite long case of the mth stage, Port 3 which also has the same impedance as the inner line of the mth stage Blumlein line can completely absorb the incident waves in the mth stage line at z_m port. Through monitoring the amplitude

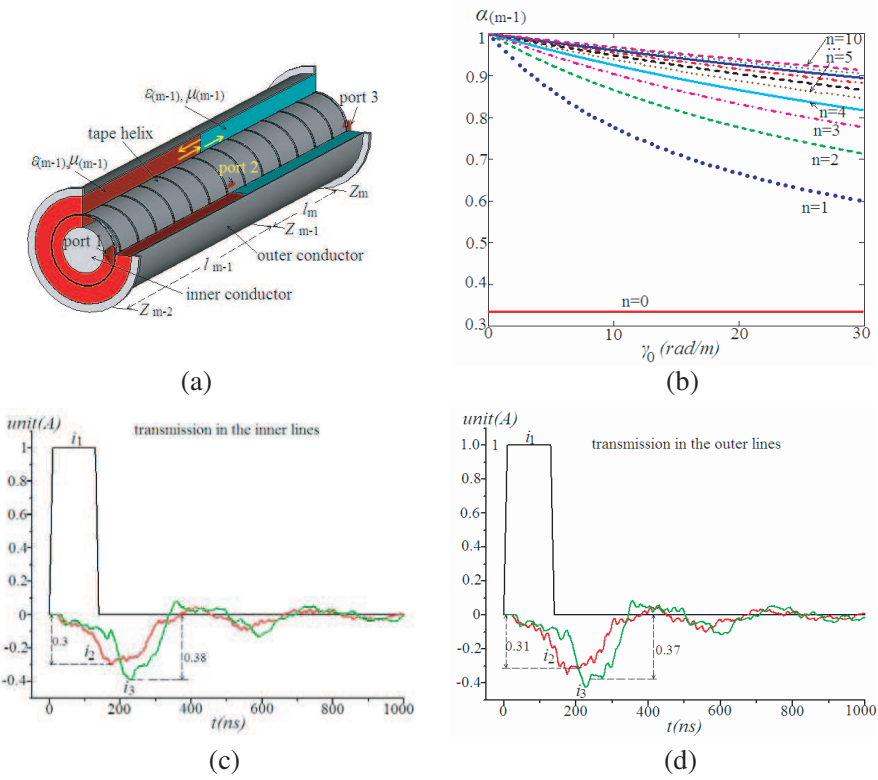

Figure 6. Comparison of the theoretical calculation result and the CST simulation results; (a) Simulation model of two stages of tape-helix Blumlein transmission lines in series; (b) Theoretical results of $\alpha_{(m-1)}$ from the dispersive propagation theory put forward in this paper; (c) CST simulation results of $\alpha_{(m-1)}$ in the inner line of the Blumlein transmission lines; (d) CST simulation results of $\alpha_{(m-1)}$ in the outer line of the Blumlein transmission lines.

of the current transmission wave i_2 at Port 2, the ratio i_2/i_1 is the transmission coefficient $\alpha_{(m-1)}$ or the S-parameter $S_{21(m-1)}$. That's to say, $i_2/i_1 = \alpha_{(m-1)} = S_{21(m-1)}$, according to (18).

According to (9) and (15), theoretical calculation results of $\alpha_{(m-1)}$ at Port 2 ($z = z_{m-1}$) is shown in Fig. 6(b). $\alpha_{(m-1)}$ of the 0th harmonic is about 0.33 while $\alpha_{(m-1)}$ of the higher order harmonics ranges from 0.6 to 1. If the calculation is in line with (17), the result is that $T_w \approx 0.33$, which demonstrates that the 0th harmonic is dominant in the current wave and electromagnetic wave. As a result, the transmission coefficient of the current wave at Port 2 is

$\alpha_{(m-1)} = S_{21(m-1)} = 0.33$. Simulation was carried out in accordance with the model shown in Fig. 6(a), and the obtained exciting current pulse i_1 at Port 1, the transmission pulse i_2 and i_3 at Port 2 and Port 3 are shown in Fig. 6(c), respectively. After the pulse delay of an electric length of the $(m-1)$th Blumlein line, pulse i_1 propagates to Port 2 and pulse i_2 forms. After about an electric length of the mth Blumlein line, pulse i_2 propagates to Port 3 and pulse i_3 forms. In line with the fixed directions of the ports set in simulation, the obtained transmission current pulses in simulation are as $i_2 = -0.3\,\mathrm{A}$ and $i_3 = -0.38\,\mathrm{A}$. i_2 and i_3 have pulse droops and ripples at the top of the pulse, which reveals that the dispersion of helical line does have effect on the travelling waves. i_2 and i_3 almost have the same pulse waveforms which demonstrates that the mth transmission line can propagate waves without any pulse deformation when the impedance is matched at Port 3. From the simulation results of i_2, the amplitude ratio of i_2 andi_1 is about 0.3, and this result is close to the theoretical calculation result $\alpha_{(m-1)} = S_{21(m-1)} = 0.33$.

In order to simulate the travelling waves propagating in the outer lines ($r_2 < r < r_3$) of the two stages of helical Blumlein lines, Port 1, Port 2 and Port 3 shown in Fig. 6(a) are reset in the outer lines at $z = z_{m-2}$, $z = z_{m-1}$ and $z = z_m$ respectively, and the positive directions of the three ports are all from the tape helix to the outer conductor. The parameters of the exciting current i_1 at Port 1 remain the same. The impedances of Port 2 and Port 3 are both set as $32\,\Omega$ to match with the impedance of the outer line ($r_2 < r < r_3$) of the mth helical Blumlein transmission line. Other parameters all remain unchanged from the simulation of Fig. 6(a). According to the proposed dispersive propagation theory and the given geometric parameters, the theoretical result that $\alpha_{(m-1)} = S_{21(m-1)} = 0.33$ is also correct to the outer lines of the two stages of Blumlein transmission lines. From the simulation, the exciting current pulse i_1 and the obtained transmission current pulses such as i_2 and i_3 at port 2 and Port 3 are shown in Fig. 6(d). The obtained transmission current pulses in simulation are as $i_2 = -0.31\,\mathrm{A}$ and $i_3 = -0.37\,\mathrm{A}$. Pulse waveforms of i_2 and i_3 are basically the same. From the simulation results shown in Fig. 6(d), the amplitude ratio of i_2 and i_1 is about 0.31 which is also close to the theoretical result $\alpha_{(m-1)} = S_{21(m-1)} = 0.33$.

The analyses and results of Fig. 6 are all based on the single-port exciting model in which only one port plays as the wave excitation port in the inner lines or in the outer lines. These simulation results include the effect of the outer lines on the waves propagating in the inner lines, or include the effect of the inner lines on the waves propagating in the outer lines. However in many practical cases, electromagnetic

waves are excited to propagate in the inner lines and the outer lines simultaneously. The simulation model in Fig. 6(a) is also improved and 6 discrete ports are used in the inner lines and outer lines. That's to say, Port 1, Port 2 and Port 3 are the same as which shown in Fig. 6(a) in the new model, while Port 4, Port 5 and Port 6 are set in the outer lines at $z = z_{m-2}$, $z = z_{m-1}$ and $z = z_m$ respectively. The settings of Port 4, Port 5 and Port 6 remain the same as the settings in the simulation corresponding to Fig. 6(d). Port 1 and Port 4 at z_{m-2} are two current exciting ports for the inner lines ($r_1 < r < r_2$) and the outer lines ($r_2 < r < r_3$) respectively. i_1 and i_4 are two quasi-square current pulses set on Port 1 and Port 4 respectively. i_1 and i_4 are completely the same with amplitude at 1 A, rise time and fall time at 10 ns, and flat top time at 110 ns. Port 2 (32 Ω) and Port 5 (32 Ω) are two impedance ports at z_{m-1} in the inner line ($r_1 < r < r_2$) and outer line ($r_2 < r < r_3$) respectively. Port 3 (32 Ω) and Port 6 (32 Ω) are also two impedance ports at z_m in the inner line ($r_1 < r < r_2$) and outer line ($r_2 < r < r_3$) respectively. Define the transmission current of Port 2, Port 3, Port 5 and Port 6 are as i_2, i_3, i_5 and i_6 respectively. Through monitoring i_2 and i_5 at z_{m-1} simultaneously, $\alpha_{(m-1)}$ and $S_{21(m-1)}$ at Port 2 and Port 5 can be obtained.

The simulation results are shown in Fig. 7. The waveforms of i_2 and i_3 are basically the same, with a pulse delay time of the electric length of the mth stage line. i_5 and i_6 basically have the same waveforms, and the pulse delay time between each other is also an electric length of the mth stage line. i_2 and i_5 are synchronous, so do i_3 and i_6. The amplitudes of i_5 and i_6 are both at 0.35 A, while the amplitudes of i_2 and i_3 are both at 0.3 A as shown in Fig. 7. The pulse amplitudes of the exciting current i_1 and i_4 are both at 1 A. The amplitude ration of i_2 and i_1 in simulation is about 0.3, while the ratio of i_5 and i_4 is about 0.35. That's to say, $\alpha_{(m-1)}$ and $S_{21(m-1)}$ of the inner line is about 0.3, while $\alpha_{(m-1)}$ and $S_{21(m-1)}$ of the outer line is about 0.35. These simulation results basically correspond to the theoretical result of 0.33 from Fig. 6(b). The designed inner lines almost have the same transmission characteristics as that of the outer lines in the helical Blumlein transmission lines.

The simulation results show that the theoretical calculation and simulation results of $S_{21(m-1)}$ parameter at z_{m-1} port correspond with each other. The good correspondence demonstrates that the proposed dispersive propagation theory is correct and reliable for the calculation of the transmission matrix and S-parameter matrix of the travelling electromagnetic waves in multiple stages of helical Blumlein transmission lines.

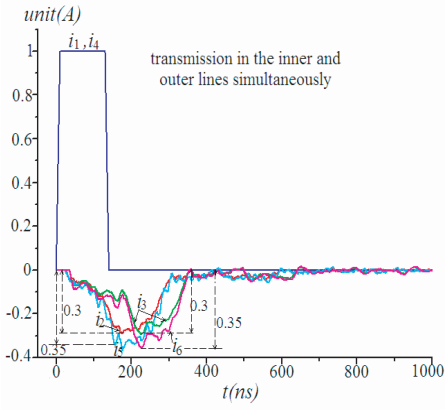

Figure 7. CST simulation results of $\alpha_{(m-1)}$ of the inner and outer lines when the input ports of the inner and the outer lines are excited by quasi-square current pulses simultaneously.

6. DEMONSTRATION EXPERIMENTS

In this section, the propagation characteristics of a single-stage helical Blumlein transmission line are demonstrated under the pulse forming model. In the pulse forming model, a load resistor R_{load} was introduced to connect with the terminal port of the single-stage Blumlein line. Through regulating R_{load}, the transmission characteristics at the terminal ports of the Blumlein line can be tested and demonstrated. The equivalent structure of the experimental setup is shown in Fig. 8(a). Before the pulse forming course, the switch which was connected with the tape helix was open, and the helical Blumlein transmission line can be charged as two capacitors with the same charging voltage as U_c. The outer conductor was connected with ground, while the inner conductor was also grounded through the load resistor R_{load}. When the switch closed, current waves flowed along the tape helix and electromagnetic wave was generated simultaneously. When the waves propagated to the terminal ports of the inner and outer lines, wave reflection and transmission phenomenon occurred. The geometric parameters of the single-stage helical Blumlein line were as $r_1 = 65\,\text{mm}$, $r_2 = 100\,\text{mm}$, $r_3 = 152\,\text{mm}$, $\delta = p = 92\,\text{mm}$ and $\psi = 81.7°$. High-voltage withstanding castor oil was employed as the filling dielectric in the Blumlein line, and ε_r=4.5, $\mu_r = 1$. Under the dominant basic harmonic condition, characteristic impedances of the inner line (region I) and the outer line (region II) can be calculated as $Z_{in} = Z_{out} = 80\,\Omega$, according to the tape-helix dispersion theory in [33]. The total impedance of the Blumlein line defined as Z_B was

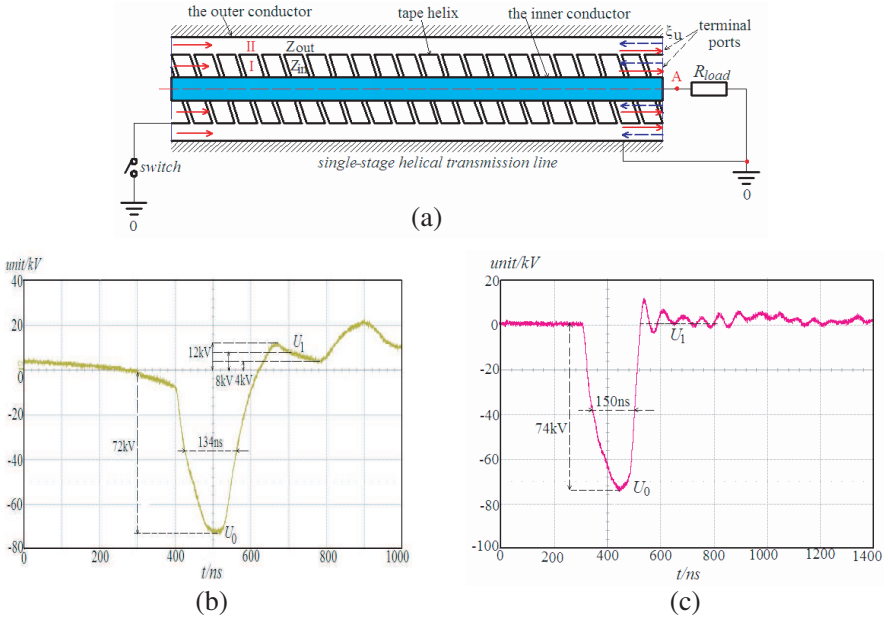

Figure 8. Equivalent structure of the experimental setup and results obtained in experiments for demonstration; (a) The equivalent structure of the experimental setup of the single-stage tape-helix Blumlein transmission line; (b) The experimental waveform on load when the load can not match with the impedance of the Blumlein transmission line; (c) The experimental waveform on load when the load matched with the impedance of the Blumlein transmission line.

as $Z_B = Z_{in} + Z_{out} = 160\,\Omega$.

If R_{load} was unmatched with Z_B, the waves repetitively reflected and transmitted at the terminal ports of the Blumlein line. As a result, oscillations appeared in the pulse tail after the main pulse was formed on R_{load}. The oscillation pulses and the main pulse almost had the same pulse duration. Define the voltage amplitude of the main pulse formed on R_{load} as U_0, and the voltage amplitude of the first oscillation pulse as U_1. According to the propagation theory under the dominant basic harmonic condition, the reflection coefficient ξ_u and the transmission coefficient α_u of the inner line at port A can be

extrapolated as

$$\begin{aligned}\xi_u &= \frac{(R_{load}+Z_{out})-Z_{in}}{(R_{load}+Z_{out})+Z_{in}} \\ &= \frac{Z_{in}}{R_{load}} - \frac{U_1}{U_0}\frac{(R_{load}+Z_{in}+Z_{out})(R_{load}+Z_{in})}{R_{load}^2}, \\ \alpha_u &= 1+\xi_u.\end{aligned} \tag{30}$$

(30) reveals that ξ_u and α_u can be easily demonstrated in experiment through measuring U_0 and U_1. When $R_{load} = 220\,\Omega$, ξ_u can be calculated from the first equation in (30), and the result is $\xi_u = 220/(220+80+80) = 57.9\%$.

Experiment was carried out when $R_{load} = 220\,\Omega$ ($R_{load} > Z_B$), and the load voltage pulse formed at point A is shown in Fig. 8(b) in the impedance-mismatching condition. A quasi-square voltage pulse was formed on R_{load} as the main voltage pulse, with full width at half maximum (FWHM) of 134 ns, and amplitude U_0 of 72 kV. The band width of the formed quasi-square pulse ranged from 0 to about 10 MHz. The quasi-square pulse waveform proved that the helical dispersion had little effect on the wave transmission and pulse forming under low frequency band, and the dominant basic harmonic condition was satisfied. The maximum value of the first oscillation pulse amplitude U_1 was about 12 kV while the minimum value of U_1 was only about 4 kV. Through averaging the maximum value and the minimum value, U_1 was about 8 kV. From the experimental results, $U_1/U_0 = 11.1\%$. Through combining U_1/U_0 and (30), $\xi_u = 62.5\%$ which basically corresponded with the theoretical calculation result 57.9%.

Under the impedance matching condition that $R_{load} = 160\,\Omega = Z_{in} + Z_{out}$, $\xi_u = 1/2$ and $U_1/U_0 = 0$ can both be obtained from (30) in theory. In experiment, the task was to demonstrate the theoretical result $U_1/U_0 = 0$ or $U_1 = 0$. Experiment was also carried out when $R_{load} = 160\,\Omega$, and the load voltage pulse formed at point A is shown in Fig. 8(c) under the impedance matching condition. The rise time of the main pulse was prolonged and the FWHM was about 150 ns. Obviously, if the dispersion had strong effect on low-frequency wave transmission, no quasi-square pulse can be obtained, because the wave components with different frequencies had different phase velocities. However, experimental result showed that quasi-square pulse was formed on the load. It demonstrated the fact again that the dominant basic harmonic condition was satisfied and the dispersion had little effect on wave transmission under low-frequency band. After the main pulse, the voltage of the pulse tail was close to 0. From the load voltage pulse, $U_0 = 74$ kV while the average of U_1 was about 0. The obtained experimental result that $U_1 \approx 0$ was proved, and

the theoretical results such as $\xi_u = 1/2$ and $U_1/U_0 = 0$ were both demonstrated under the impedance matching condition.

7. CONCLUSION

In this paper, a set of fully dispersive propagation theory based on matrix method is firstly introduced to explain the propagation characteristics of travelling electromagnetic waves in multiple stages of helical Blumlein transmission lines with finite lengths. As a useful innovation, the proposed fully dispersive propagation theory can independently analyze the wave propagation issues without considering the lumped circuit theory. The effects of dispersion and dielectrics on the propagation matrix and S-parameter matrix of the travelling waves are analyzed in detail. The study reveals that the dispersion has weak effect on the transmission and reflection coefficients of the basic harmonic component of electromagnetic wave, while these coefficients of the higher order harmonic components of electromagnetic wave are strongly affected. As a result, the high-frequency electromagnetic waves which are largely contributed by the higher order harmonics are obviously affected by dispersion when travelling in the helical transmission lines. In the low frequency band, the electromagnetic waves are mainly contributed by the basic harmonic wave so that the dispersion effect on the propagation characteristics of the helical transmission lines is weak. At each port of helical lines, the transmission matrix and S-parameter matrix are completely determined by the dielectric permittivities and the dispersion relation of the helical lines.

ACKNOWLEDGMENT

This work is supported by the National Natural Science Foundation of China under Grant No. 51177167. It is also supported by the Fund of Innovation, Graduate School of National University of Defense Technology under Grant No. B100702. Furthermore, the work is supported by Hunan Provincial Innovation Foundation for Postgraduate under Grant No. CX2010B034.

REFERENCES

1. Suh, J. D., M. E. Hardy, and A. Ardalan, "Measurements of communication signal propagation on three phase power distribution lines," *IEEE Transactions on Power Delivery*, Vol. 6, No. 3, 945–951, Mar. 1991.

2. Jiang, X., Y. Xia, J. Hu, F. Yin, C. Sun, and Z. Xiang, "Optimal design of MFL sensor for detecting broken steel strands in overhead power line," *Progress In Electromagnetics Research*, Vol. 121, 301–315, 2011.
3. Wang, W., P. G. Liu, and Y. J. Qin, "An unconditional stable 1D-FDTD method for modeling transmission lines based on precise split-step scheme," *Progress In Electromagnetics Research*, Vol. 135, 245–260, Jan. 2013.
4. Deng, P.-H., J.-H. Guo, and W.-C. Kuo, "New Wilkinson power dividers based on compact stepped-impedance transmission lines and shunt open stubs," *Progress In Electromagnetics Research*, Vol. 123, 407–426, 2012.
5. Wu, Y. and Y. Liu, "A coupled line band-stop filter with three section transmission line stubs and wide upper pass-band performance," *Progress In Electromagnetics Research*, Vol. 119, 407–421, Aug. 2011.
6. Liu, Y., L. Tong, W. Zhu, Y. Tian, and B. Gao, "Impedance measurements of nonuniform transmission lines in time domain using an improved recursive multiple reflection computation method," *Progress In Electromagnetics Research*, Vol. 117, 149–164, 2011.
7. Silapunt, R. and D. Torrungrueng, "Theoretical study microwave transistor amplifier design in the conjugately characteristic impedance transmission line (CCITL) system using a bilinear transformation approach," *Progress In Electromagnetics Research*, Vol. 120, 309–326, 2011.
8. Mujumdar, M. D., J. Cheng, and A. Alphones, "Double periodic composite right/left handed transmission line based leaky wave antenna by singular perturbation method," *Progress In Electromagnetics Research*, Vol. 132, 113–128, 2012.
9. Yang, J., T. Shu, and J. Zhang, "Time-resolved plasma characteristics in a short-pulse high-power diode with a dielectric fiber (velvet) cathode," *IEEE Transactions on Plasma Science*, Vol. 40, No. 6, 1696–1700, Jun. 2012.
10. Li, J., X. Li, and X. P. Liu, "Some design approaches to a MHz repeating rate burst high-voltage generator," *Second European Pulsed Power Symposium*, 155–158, 2004.
11. Li, J., X. Li, and X. P. Liu, "MHz repetition rate pulsed power technology," *High Power Laser and Particle Beams*, Vol. 22, No. 4, 725–729, Apr. 2010 (in Chinese).
12. Kirbie, H., G. Coporaso, and D. Goerz, "MHz repetition rate solid-state driver for high current induction accelerators," *Particle*

Accelerator Conference, 423–427, 1999.

13. Chen, S. F., J. J. Deng, and X. Li, "Design and characterization of a high-power induction module at megahertz repetition rate burst mode," *Nuclear Instruments and Methods in Physics Research A*, Vol. 579, 941–950, 2007.
14. Hegeler, F., M. W. McGeoch, J. D. Sethian, H. D. Sanders, S. C. Glidden, and M. C. Myers, "A durable gigawatt class solid state pulsed power system," *IEEE Transactions on Dielectrics and Electrical Insulation*, Vol. 18, No. 4, 1205–1213, Apr. 2011.
15. Lindblom, A., H. Bernhoff, and J. Isberg, "An inductive 700-MW high-voltage pulse generator," *IEEE Transactions on Plasma Science*, Vol. 34, No. 5, 1838–1845, May 2006.
16. Davanloo, F., C. B. Collins, and F. J. Agee, "High-power, repetitive-stacked Blumlein pulsers commutated by a single switching element," *IEEE Transactions on Plasma Science*, Vol. 26, No. 5, 1463–1475, May 1998.
17. Feng, T., Y. Li, H. Jiang, W. Li, F. Yang, X. Dong, and H. Chen, "Tunable single-negative metamaterials based on microstrip transmission line varactor diodes loading," *Progress In Electromagnetics Research*, Vol. 120, 35–50, 2011.
18. Sheu, T. W. H., R. Y. Chung, and J. H. Li, "Development of a symplectic scheme with optimized numerical dispersion-relation equation to solve Maxwell's equations in dispersive media," *Progress In Electromagnetics Research*, Vol. 132, 517–549, Oct. 2012.
19. Liu, L. W., Y. Y. Wei, and J. Xu, "A novel slotted helix slow-wave structure for millimeter-wave travelling-wave tube," *Progress In Electromagnetics Research*, Vol. 135, 347–362, Jan. 2013.
20. Teranishi, T., K. Nojima, and S. Motegi, "A 600 kV Blumlein modulator for an X-band klystron," *The 8th IEEE International Pulsed Power Conference*, 315–318, 1991.
21. Liu, J. L., X. B. Cheng, and B. L. Qian, "Study on strip spiral Blumlein line for the pulsed forming line of intense electron-beam accelerators," *Laser and Particle Beams*, Vol. 27, No. 1, 95–105, Jan. 2009.
22. Korovin, S. D., I. K. Kurkan, and S. V. Loginov, "Decimeter-band frequency-tunable sources of high-power microwave pulses," *Laser and Particle Beams*, Vol. 21, 175–185, 2003.
23. Sethian, J. D., M. Myers, and J. L. Giuliani, "Electra: A repetitively pulsed, electron beam pumped KRF laser to develop the technologies for fusion energy," *IEEE Pulsed Power*

Conference, 8–15, 2005.

24. Boyko, I. M., "Helix antennas for generators of short high-voltage pulses," *Internal Conference on Antenna Theory and Techniques (IEEE)*, 140–142, Sep. 2007.
25. Akiyama, H., T. Sagugawa, and T. Namihira, "Industrial applications of pulsed power technology," *IEEE Transactions on Dielectrics and Electrical Insulation*, Vol. 14, No. 5, 1051–1064, May 2007.
26. Dong, J. F. and J. Li, "The reflection and transmission of electromagnetic waves by a uniaxial chiral slab," *Progress In Electromagnetics Research*, Vol. 127, 389–404, May 2012.
27. Asad, H., M. Zubair, and M. J. Mughal, "Reflection and transmission at dielectric-fractal interface," *Progress In Electromagnetics Research*, Vol. 125, 543–558, Mar. 2012.
28. Cheng, X. B., J. L. Liu, B. L. Qian, and J. D. Zhang, "Effect of transition section between the main switch and middle cylinder of Blumlein pulse forming line on the diode voltage of intense electron-beam accelerators," *Laser and Particle Beams*, Vol. 27, No. 3, 439–447, Mar. 2009.
29. Cheng, X. B., J. L. Liu, and Y. Zhang, "Effect of a transition section between the Blumlein line and a load on the output voltage of gigawatt intense electron-beam accelerators," *Physical Review Special Topics-accelerators and Beams*, Vol. 12, 110401, Dec. 2009.
30. Cheng, X. B., J. L. Liu, and Z. Q. Hong, "Operating characteristics of intense electron beam accelerator at different load conditions," *Laser and Particle Beams*, Vol. 30, No. 4, 531–539, Apr. 2012.
31. Zhang, Y., J. L. Liu, and J. H. Feng, "Effects of dispersion on electromagnetic parameters of tape-helix blumlein pulse forming line of accelerator," *The European Physical Journal Applied Physics*, Vol. 57, No. 3, 30904, Mar. 2012.
32. Zhang, Y., J. L. Liu, and X. L. Fan, "Characteristic impedance and capacitance analysis of Blumlein type pulse forming line based on tape helix," *Review of Scientific Instruments*, Vol. 82, No. 10, 104701, Oct. 2011.
33. Zhang, Y., J. L. Liu, and S. W. Wang, "Effects of dielectric discontinuity on the dispersion characteristics of the tape helix slow-wave structure with two metal shields," *Laser and Particle Beams*, Vol. 29, 459–469, Oct. 2011.
34. Sensiper, S., "Electromagnetic wave propagating on helical structures (a review of survey of recent progress)," *Proceedings of the IRE*, Vol. 43, 149–161, 1955.